Pairwise and Higher-Order measures of Brain-Heart Interactions in Children with Temporal Lobe Epilepsy

Riccardo Pernice[1], Luca Faes[1,*], Martha Feucht[2], Franz Benninger[3], Stefano Mangione[1], Karin Schiecke[4]
[1]*Department of Engineering, University of Palermo, Palermo, Italy*
[2]*Epilepsy Monitoring Unit, Department of Paediatrics, Medical University Vienna, Vienna, Austria*
[3]*Department of Child and Adolescent Medicine, Medical University Vienna, Vienna, Austria*
[4]Institute of Medical Statistics, Computer and Data Sciences, Jena University Hospital, Friedrich Schiller University Jena, Jena, Germany

Email:
*luca.faes@unipa.it

Received
Accepted for publication
Published

Abstract

Objective: While it is well-known that epilepsy has a clear impact on the activity of both the central nervous system (CNS) and the autonomic nervous system (ANS), its role on the complex interplay between CNS and ANS has not been fully elucidated yet. In this work, pairwise and higher-order predictability measures based on the concepts of Granger causality (GC) and Partial Information Decomposition (PID) were applied on time series of electroencephalographic (EEG) brain wave amplitude and heart rate variability (HRV) in order to investigate directed brain-heart interactions associated with the occurrence of focal epilepsy.
Approach: HRV and the envelopes of δ and α EEG activity recorded from ipsilateral (ipsi-EEG) and contralateral (contra-EEG) scalp regions were analyzed in 18 children suffering from temporal lobe epilepsy monitored during pre-ictal, ictal and post-ictal periods. After linear parametric model identification, we compared pairwise GC measures computed between HRV and a single EEG component with PID measures quantifying the unique, redundant and synergistic information transferred from ipsi-EEG and contra-EEG to HRV.
Main results: The analysis of GC revealed a dominance of the information transfer from EEG to HRV and negligible transfer from HRV to EEG, suggesting that CNS activities drive the ANS modulation of the heart rhythm, but did not evidence clear differences between δ and α rhythms, ipsi-EEG and contra-EEG, or pre- and post-ictal periods. On the contrary, PID revealed that epileptic seizures induce a reorganization of the interactions from brain to heart, as the unique predictability of HRV originated from the ipsi-EEG for the δ waves and from the contra-EEG for the α waves in the pre-ictal phase, while these patterns were reversed after the seizure.
Significance: These results highlight the importance of considering higher-order interactions elicited by PID for the study of the neuro-autonomic effects of focal epilepsy, and may have neurophysiological and clinical implications.

Keywords: Granger Causality (GC), Linear prediction, Multivariate Time Series Analysis, Epilepsy, Heart Rate Variability, Information Dynamics.

Introduction

Epilepsy is a brain disorder characterized by recurrent and unpredictable interruptions of the normal brain function manifested through the occurrence of epileptic seizures [1]. Epilepsy has been demonstrated to influence both the central nervous system (CNS) and the autonomic nervous system (ANS) activities, as well as the coupling between them [1–5]. Seizures episodes usually produce redundant hyper-synchronous activity of neurons in the brain causing CNS disorders reflected by altered patterns of brain connectivity, typically assessed through cortical electroencephalographic (EEG) waves [1,4] or more recently also through resting state functional Magnetic Resonance Imaging (fMRI) or combined EEG–fMRI acquisitions [6,7]. The changes in ANS activity are mostly assessed through heart rate variability (HRV) analysis [8–10], and different HRV indexes have been proposed in time, frequency, and information-theoretic domains to detect ANS alterations in relation to the type of epilepsy and to the evolution of the epileptic seizure [2,3,5].

In both healthy subjects and epileptic patients, the brain and cardiovascular systems exhibit a strong interplay, also known as brain-heart interaction, which reflects homeostasis as well as a number of physiological functions [11–14]. This functional interplay results from the fact that, anatomically, the heart has extensive efferent and afferent neural connections with the brain [14]. A key role in brain-heart interactions is played by the sympathetic and parasympathetic control carried out on cardiovascular dynamics [12,13], mainly by sympathetic post-ganglionic fibers. On the other side, cardiac afferent inputs to the brain influence the activity of brain areas involved in perceptual and cognitive processing [14]. Imbalanced brain–heart interactions can have potential clinical implications and thus a negative impact on health, which may include cerebrovascular and cardiovascular diseases, but also psychiatric and neurological disorders. Given the effects of epileptic seizures on both ANS and brain oscillations, an increasing interest has been devoted to the study of brain-heart interactions in epilepsy [15–18]. In particular, previous studies have demonstrated that seizures may provoke a wide range of transient cardiac effects, ranging from variations in heart rate and HRV to arrhythmias, and asystole; such cardiac abnormalities could play a significant role for sudden unexpected death in epilepsy (SUDEP) during and between seizures [12,15,19].

The evaluation of ANS/CNS interactions can be framed within the general field of "network physiology", in which the human body is interpreted as an integrated network where multiple organs continuously interact with each other reflecting different physiological and pathological states [20,21]. In this context, new possibilities to analyze the dynamic activity of the human physiological network have emerged with recent advances in the analysis of multivariate physiological time series. A vast number of analytical and computational approaches have been recently developed to characterize brain-heart interactions. These approaches are specifically devised to quantify the functional coupling between two synchronized time series, one representing the CNS and the other the ANS [11,12,22–30]. The methods developed include simple pairwise linear correlation metrics such as the Pearson's correlation coefficient [24–26], time-delay stability linked to the maximum cross-correlation function between the two systems [20], coupling and coherence measures such as synchronization likelihood [27], the Maximal Information Coefficient quantifying linear and nonlinear coupling between concurrent brain–heart outflows [23,28], Joint Symbolic Analysis [29], Convergent Cross Mapping (CCM) assessing bivariate directed nonlinear interactions between dynamical systems [31], or even synthetic data generation models [22,30].

Additionally, principles from the field of information theory (e.g., the so-called framework of information dynamics) [32] can be exploited, also with regard to brain-heart interactions, to assess how multiple physiological processes are interrelated evidencing aspects that go beyond the simple pairwise interaction between two processes [33–39]. In fact, while well-established tools like Granger Causality (GC) assess pairwise directional interactions between two subsystems of a complex system [40,41], emerging approaches to multivariate analysis are focused on detecting interactions among several subsystems that cannot be otherwise described by pairwise links, i.e. the so called "higher-order" interactions. High-order interdependencies are at the core of complex systems, and play a key role for the multivariate description of many biological systems where pairwise interactions fail to describe emergent behaviors which arise as a consequence of the interplay among more than two network nodes [42–46]. Of note, high-order interactions should not be confused with higher-order statistics (HOS), i.e. moments and cumulants of third order and beyond, which can detect deviations from linearity, stationarity or Gaussianity in a signal and that have been widely employed for analyzing biomedical signals and also brain-heart interactions [47–49].

Among the approaches for the analysis of higher-order interactions [33,34,42–46,50], the so-called "partial

information decomposition" (PID) [33] is employed to decompose, in a network of multiple physiological processes, the information flowing from two sources to a target into unique contributions related to each individual source and separate synergistic and redundant contributions that reflect the nature of source interactions [34,50]. The focus of the present work is on the use of PID for investigating the effects of epileptic seizures on directed brain-heart interactions in children with temporal lobe epilepsy (TLE). Implementing a linear parametric formulation of the PID measures, we evaluate from a new perspective the role played by different EEG waves in contributing to the neuro-autonomic control of brain-heart interactions during epilepsy, analyzed in previous works with different methods [5,17,18,31,51]. The choice to analyze the separate and combined effects between ipsilateral and contralateral EEG components with regard to their communication with HRV is motivated by the intention to investigate the combined effects that brain waves located in regions very close (i.e. in ipsilateral region) and far away (i.e. in contralateral region) from the epileptic focus have on the rhythm of the cardiac pacemaker. This analysis entails evaluation of higher-order interactions analyzed by PID, in the specific case related to the synergistic and redundant efferent modulations of the activity at the sinus node driven by brain regions located ipsi- and contra-laterally to the seizure site.

In epilepsy, until now the study of brain-heart interactions has been performed through the utilization of several linear and nonlinear analyses of time-variant coherence and synchronization between HRV and EEG components, with the goal of evaluating the effects of seizure activity on the coupling between CNS and ANS dynamics [5,15,17,31]. In a previous study [31], computation of the bivariate CCM index has been performed to study time-resolved directed brain-heart interactions between HRV and specific EEG rhythms. Here, we overcome the bivariate nature of CCM implementation to explore more thoroughly the joint ANS and cortical modulations with the application of multivariate GC and PID on the dynamics of site-specific EEG activity and of HRV measured before, during and after seizures in children affected by TLE.

Materials and methods

2.1 Data acquisition

The study was carried out using a dataset previously acquired and employed for other studies, e.g. to explore brain-heart interactions through the CCM method [31]. In the present work, these data will serve as benchmark data for a comparison of our methods to bivariate methods like CCM.

The data were extracted from ongoing recordings accompanied by video records performed for presurgical evaluation within the standard clinical setting of the Epileptic Monitoring Unit (EMU) in Vienna pediatric epilepsy center. During the recordings, the children were sitting/lying in their beds, and thus were restricted by their recording devices but able to move more or less freely.

The data were recorded on 18 children (7 male, 11 female) suffering from TLE; the median age was 9.4 years (interquartile range 3.37 years, minimal age 6.5 years, maximal age 18 years). The group of 18 patients was divided according to the side of the seizure focus, i.e. left or right hemispheric TLE, with 9 patients belonging to each sub-group. The median duration of the seizures was 88 s (interquartile range 35 s, minimal length of seizure 52 s and maximal length 177 s). The protocol was approved by the local ethical committee of the University Hospital of Vienna.

Data consisted of electrocardiographic (ECG) and electroencephalographic (EEG) recordings. For each child, one-lead ECG was acquired through an electrode placed under the left clavicle, and 23-channels EEGs were acquired from gold disc electrodes located according to the extended 10–20 system with additional temporal electrodes [31] (see Figure 1(a)). Both ECG and EEG signals were recorded referentially against the electrode position CPZ with sampling frequency of 256 Hz and then underwent bandpass filtering (1-70 Hz). Additional details on data acquisition protocol can be found in [31], while further information about the classification of seizure type, onset and termination are reported in Ref. [52].

2.2 Data processing and time series extraction

The analyzed data consisted of power EEG and HRV time series extracted from EEG and ECG recorded synchronously on the 18 epileptic children starting 5 minutes before (pre-ictal period) up to 5 minutes after the seizure onset (ictal and post-ictal periods).

In order to detect the QRS complexes, the ECG signals were first band-pass filtered (10-50 Hz) and then interpolated (cubic spline algorithm, 1024 Hz). Afterwards, the R peaks were extracted as the time of the maximum amplitude of each R-wave [31]; a manual procedure of artifact rejection was carried out to avoid false QRS detection. The R-R time series were then obtained as the sequence of the temporal differences between consecutive detected R peaks. Subsequently, to obtain time series sampled at equal intervals, the French-Holden algorithm was applied to the unevenly sampled R-R intervals; a cutoff frequency lower than half of the mean heart rate (HR) was used in this step [53]. The HRV representation was obtained via multiplication of the low-pass filtered series of events with the sampling rate and with 60 beats per minute, and finally downsampled to 8 Hz [31,53]. An exemplary HRV time series obtained using through this procedure is shown in Figure 1(b).

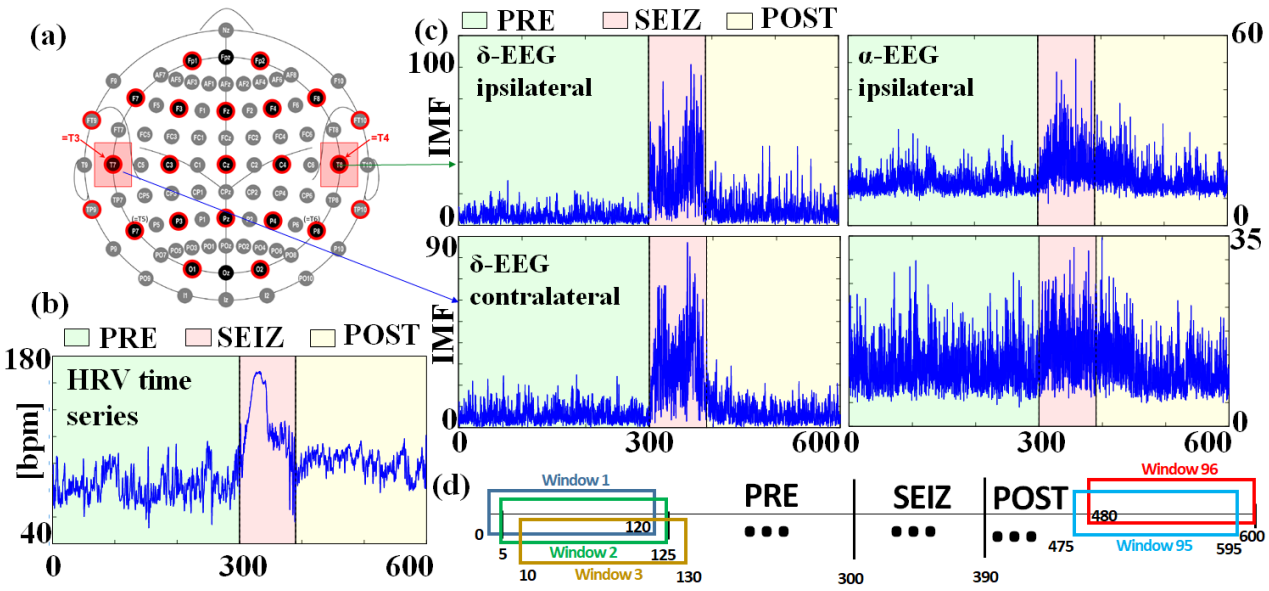

FIGURE 1. Schematic representation of the experimental protocol and exemplary time series. (a) EEG electrodes locations, where T3 and T4 indicate temporal electrodes considered for the analysis (in the example: child with left-side seizure, so that T3 is the ipsilateral and T4 the contralateral electrode); (b) Exemplary HRV time series; and (c) EEG-IMFs time series of ipsilateral and contralateral δ and α EEG; (d) Schematic representation of the processing steps used for extracting the time-varying moving windows analyzed in the pre-ictal (PRE), ictal (SEIZ) and post-ictal (POST) phases.

With regard to EEG data, the acquired signals were first downsampled to 64 Hz and preprocessed through independent component analysis (ICA) to remove artifacts; we refer the readers to Ref. [5] for further details. The EEG signals recorded from the two electrodes (T3 or T4) selected at the seizure side (ipsilateral) and at the opposite side (contralateral) were processed with multivariate empirical mode decomposition (MEMD) [54] to decompose each signal into a finite number of intrinsic mode functions (IMFs); IMFs are formed by an amplitude- and frequency-modulated zero mean oscillatory signal and a monotonic residual. For subsequent analyses, only the IMFs mostly corresponding to the standard δ EEG band (IMF4) and to the α band (IMF2) were selected. Their envelopes were computed (with sampling frequency of 8 Hz) for all channels and for every patient using the Hilbert transform. Exemplary time series of IMFs of δ and α EEG band measured from ipsilateral and contralateral electrodes are depicted in Figure 1(c). We refer the reader to Ref.[5] for further details on the MEMD approach and the computation of envelopes of IMFs.

The time series used for the computation of the prediction measures described in the following subsection were:

- one 10 min HRV time series per child (sampled at 8 Hz)
- one 10 min times series of EEG components (envelopes of EEG-IMFs) per child in the δ and α bands recorded at temporal electrodes placed both ipsilaterally and contralaterally with respect to the seizure focus (sampling frequency = 8 Hz).

Before computing the prediction measures, the α and δ time series, as well as the HRV series (herein referred as η) were normalized to zero mean and unit variance. A time-varying moving window based approach was employed to analyze the directed interactions between HRV and the specific EEG components in the pre-ictal (~ 5 min), ictal (~ 1.5 min) and post-ictal (~ 3.5 min) periods (windows selection as in Fig. 1(d) [31]). The duration of the windows was set to 120 s, while the shift forward for time-varying analysis was imposed to 5 s, thus generating 96 windows in the overall 10-minute recording. For each child, 48 windows belonged to the pre-ictal phase, 19 to the ictal phase and 29 to the post-ictal phase, respectively.

2.3 Predictability Decomposition Framework

The time series were analyzed using linear time-domain Granger causality (GC) measures, which are widely employed to infer causal interactions in complex system of many variables [41]. GC measures quantify directed interactions in terms of predictability, reflecting the directed information transfer from one or more source processes to a target. Given two stochastic processes X and Y, it is possible to say that X *Granger causes* Y if we can predict the current value of Y better using past values of Y than using past values of X alone [55]. In our setting, we consider a discrete-time, stationary vector stochastic process $\mathbf{\Omega}=\{Y,\mathbf{X}\}$ consisting of two sources (X_1 and X_2 composing $\mathbf{X}$) and one target (Y), each one represented by realizations of N samples. Let us define Y_n as

the present state of the target process, and similarly $X_{1,n}$ and $X_{2,n}$ as the present states of the two sources. We can describe Y_n as resulting from the linear combination of p past target values, and of p past values of the sources, according to the autoregressive (AR) model of order p and with two exogenous inputs [56]:

$$Y_n = \sum_{k=1}^{p} A_k Y_{n-k\tau} + \sum_{m=1}^{M} \sum_{k=1}^{p} B_{mk} X_{m,n-k\tau} + W_{\Omega,n} \ , \quad (1)$$

where M=2 (m=1,2), A_k and $B_{m,k}$ are linear regression coefficients, τ is the delay between consecutive time-lagged components taken for the regression, and W_Ω is a scalar zero mean innovation process uncorrelated with X_1 and X_2. To measure the unpredictability of Y given $\boldsymbol{\Omega}$ with the model (1), we consider the variance of W_Ω, denoted as $\sigma^2(Y|\Omega) = \sigma^2(Y|Y,\boldsymbol{X})$, which is bounded between 0 and the variance of Y, $\sigma^2(Y)$ [56]. Then, disregarding the two sources, we can describe Y as a function of its past through the following reduced linear AR model without exogenous inputs [56]:

$$Y_n = \sum_{k=1}^{\infty} \tilde{A}_k Y_{n-k\tau} + W_{Y,n} \ , \quad (2)$$

where the linear regression coefficients $\tilde{A}_k$ generally differ from the coefficients A_k in eq. (1) and where the variance $\sigma^2(Y|Y)$ of the innovation process W_Y reflects the unpredictability of the present of the target process given its past only.

Based on the above formulations, the joint Granger Causality (JGC) from the two sources X_1 and X_2 towards the target process Y is defined as:

$$F_{X_1X_2\to Y} = \sigma^2(Y|Y) - \sigma^2(Y|Y,\boldsymbol{X}), \quad (3)$$

which quantifies the amount of the variance of Y that can be predicted from the knowledge of the history of X_1 and X_2 above and beyond the knowledge of the history of the target, and thus is a measure of causal predictability of Y given $\mathbf{X}$ [56]. Similarly, we can reformulate eq. (1) to consider only Y and one source (separately X_1 or X_2) to calculate bivariate GC measures that allow to predict Y starting from its past and the past of the source taken into account:

$$F_{X_1\to Y} = \sigma^2(Y|Y) - \sigma^2(Y|Y,X_1) \ , \quad (4a)$$
$$F_{X_2\to Y} = \sigma^2(Y|Y) - \sigma^2(Y|Y,X_2) \ . \quad (4b)$$

The GC measures in eqs. (4) can be referred as "individual" causal predictability indices, since they assess the amount of the variance of Y that can be predicted from the knowledge of a given source above and beyond the amount that can be predicted when considering the target alone [56].

Starting from the concepts of causal predictability above defined, we can also investigate on how the sources interact with each other for predicting the target dynamics. Specifically, the Interaction Granger Causality (IGC) is defined as:

$$I_{X_1X_2\to Y} = F_{X_1X_2\to Y} - F_{X_1\to Y} - F_{X_2\to Y}, \quad (5)$$

which is a measure of interaction predictability, meaning that it informs about the nature of the interaction between the past states of X_1 and X_2 when they contribute to predict the present state of Y. Specifically, the IGC is positive in case of predictive synergy, i.e. when considering the two sources together produces a better prediction of the target than summing up the individual predictabilities from each source. The IGC is instead negative in the case of predictive redundancy, i.e. when a better prediction of the target dynamics is achieved keeping the sources separate than joining them together.

The IGC measure computed as in eq. (5) implements within the framework of linear prediction the approach known as interaction information decomposition (IID) [33,56]. An alternative approach to the study of higher order interactions between multivariate processes is the Partial Information Decomposition (PID), which allows to derive separate and non-negative measures of redundancy and synergy [41,56]. Here, we implement the PID in the context of linear prediction determining four distinct quantities that assess the unique predictability of the target arising from each source taken individually ($U_{X_1\to Y}$ and $U_{X_2\to Y}$) and the redundant and synergistic contributions to the target predictability arising from the sources considered together ($R_{X_1X_2\to Y}$ and $S_{X_1X_2\to Y}$). Redundancy can be defined, in the context of linear prediction, as the minimum amount of causal predictability arising from each source considered individually [57]:

$$R_{X_1X_2\to Y} = \min\{F_{X_1\to Y}; F_{X_2\to Y}\} \ ; \quad (6)$$

then, the unique GCs are derived removing the redundant contribution from each bivariate GC:

$$U_{X_1\to Y} = F_{X_1\to Y} - R_{X_1X_2\to Y} \ , \quad (7)$$
$$U_{X_2\to Y} = F_{X_2\to Y} - R_{X_1X_2\to Y} \ , \quad (8)$$

and the synergistic predictability results as the amount of predictability missed to provide the JGC:

$$S_{X_1X_2\to Y} = F_{X_1X_2\to Y} - U_{X_1\to Y} - U_{X_2\to Y} - R_{X_1X_2\to Y} \quad (9)$$

Given eqs. (6)-(8), it follows that one between $U_{X_1\to Y}$ and $U_{X_2\to Y}$ must be zero. Therefore, eq. (9) can be rewritten as:

$$S_{X_1X_2\to Y} = F_{X_1X_2\to Y} - max\{F_{X_1\to Y}; F_{X_2\to Y}\} \ . \quad (10)$$

The IID and PID measures defined respectively in eq. (5) and in eqs. (6)-(9) can be related to each other by the following relation:

$$I_{X_1X_2\to Y} = S_{X_1X_2\to Y} - R_{X_1X_2\to Y} \ , \quad (11)$$

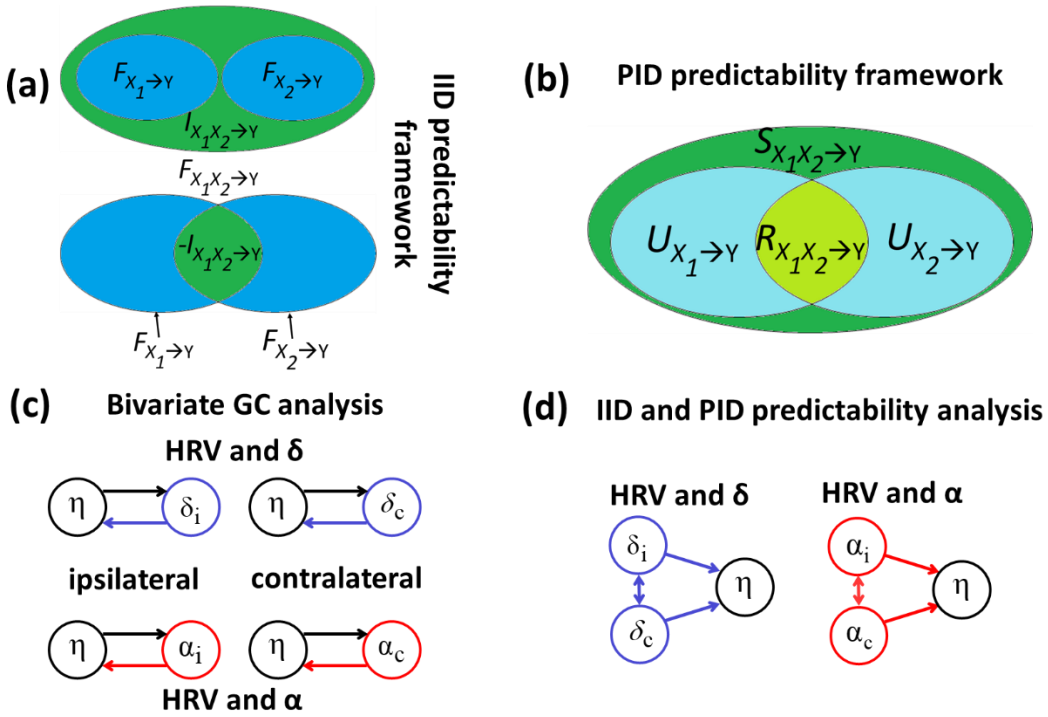

FIGURE 2. (a) Graphical representation of the IID predictability framework. The total area represents the JGC, and is split in two blue areas symbolizing the bivariate GC and a green area symbolizing the IGC, which is positive in the case of synergy (up) and negative in the case of redundancy (down). (b) Graphical representation of the PID predictability framework. The total area represents the JGC, and is split in two cyan areas symbolizing the unique GCs, a light green area symbolizing the redundant GC, and a green area symbolizing the synergistic GC; in this case all measures are positive. (c) Schematization of the application of bivariate GC to assess directed interactions between HRV and ipsilateral or contralateral δ or α EEG power; (d) Schematization of the application of IID and PID to quantify IGC as well as unique, redundant and synergistic predictability of HRV given the ipsilateral and contralateral EEG power in the δ or α bands.

showing that the IGC quantifies the balance between synergistic and redundant Granger-causal influences directed from the two sources to the target.

A graphical representation of the relations determining the IID and PID formulations with the linear predictability measures above defined is provided in Fig. 2a,b using Venn diagrams. We note that, when the considered processes X_1, X_2 and Y have a joint Gaussian distribution, the measures taken from our predictability framework are formally equivalent to the better-known information-theoretic formulations [41,56].

2.4 Application of Predictability Decomposition to data and statistical analyses

The IID and PID predictability frameworks defined in the previous section were exploited to investigate the interactions between HRV and the EEG components of interest on epileptic patients and to decompose, separately for δ and α waves, the joint and individual GC from the ipsilateral and contralateral EEG activity to HRV into unique, redundant and synergistic predictability. In detail, as schematized in Fig. 2(c) and (d), we took into account the ipsilateral and contralateral δ and α brain waves and the cardiac dynamics η, to assess the following interactions:

(a) η and δ ipsilateral (δ_i) or contralateral (δ_c): HRV and the envelope of EEG component IMF4 at the ipsilateral (T3 for N=9 children with left-side seizure or T4 for N=9 children with right-side seizure) or contralateral (T4 for N=9 children with left-side seizure or T3 for N=9 children with right-side seizure) electrode (Figure 2(c), top);

(b) η and α ipsilateral (α_i) or contralateral (α_c): HRV and the envelope of EEG component IMF2 at the ipsilateral (T3 for N=9 children with left side seizure or T4 for N=9 children with right side seizure) or contralateral (T4 for N=9 children with left-side seizure or T3 for N=9 children with right-side seizure) electrode (Figure 2(c), bottom);

(c) η and both δ ipsilateral (δ_i) and contralateral (δ_c): HRV and the envelope of EEG component IMF4 at the ipsilateral and contralateral electrodes (Figure 2(d), left);

(d) η and both α ipsilateral (α_i) and contralateral (α_c): HRV and the envelope of EEG component IMF2 at the ipsilateral and contralateral electrodes (Figure 2(d), right).

In this work we have analyzed only δ and α brain waves since previous studies on the same dataset evidenced that those represent the most prominent frequency regions of interest with respect to the epileptic activity and the most useful for assessing changes in brain-heart interactions, while considering also the θ and β frequency ranges did not provide a significant increase in information [17,31]. To perform the

above analyses, for each patient and each temporal window two vector AR (VAR) models comprising three time series were identified: a VAR model including realizations of the η, δ_i and δ_c processes, and a VAR model including realizations of the η, α_i and α_c processes. These VAR models were formulated as in eq. (1) where Y takes the role of each of the three analyzed processes, and were identified using the ordinary least squares method to find the relevant parameters; the order of each VAR model was fixed to p=8 and the delay between time-lagged components was set to $\tau = 5$, respectively in agreement with the embedding dimension and the time lag used for the nonlinear state space reconstruction in the CCM analysis in Ref. [31]. Then, after VAR identification, the partial variances needed for the computation of the GC measures in eqs. (3) and (4) and all the IID and PID measures were computed from the VAR parameters using the approach described in Ref. [58]; this approach, which makes use of the correlations between the present and the past values of the various processes (here assessed up to a lag q=20 [33,58]), is preferred to performing separate identification of the reduced model in eq. (2), since the direct identification of this infinite-order model would be unavoidably affected by the tradeoff between bias and variance encountered when setting the order [59].

For each of the 96 windows obtained according to the procedure previously described, IID and PID predictability measures were computed from the corresponding time series of α-EEG, δ-EEG and HRV. For each window, the median value across all the subjects was then computed and used to perform the statistical analyses among conditions. The statistical significance of the computed GC measures was tested using a parametric F-test, a widely-employed approach for assessing statistical differences in conditional entropies or Granger Causality measures estimated through linear regression [60,61]. Moreover, the distributions of the PID measures (unique, redundant and synergistic predictability) were compared across conditions (pre-ictal, ictal and post-ictal) using non-parametric tests, given that the hypothesis of normality was rejected for most of the distributions according to Anderson-Darling test. The non-parametric Kruskal-Wallis test was employed to assess the statistical significance of the differences of the median of the distributions among groups, followed in case of rejection by a post-hoc pairwise comparison carried out through unpaired (given the different number of windows) Wilcoxon rank sum non-parametric test with Bonferroni correction for multiple comparison (n=3) to assess the differences between pairs of distributions (pre-ictal vs ictal, pre-ictal vs post-ictal and ictal vs post-ictal). All statistical tests were carried out with 5% significance level.

Results

Figure 3 depicts the results of the computation of bivariate measures of GC to assess the directed interactions between HRV and δ or α EEG power extracted on the ipsilateral or contralateral temporal electrodes. Results indicate that the GC is high when computed in the direction from the δ or α EEG components to HRV, while it is markedly lower and close to zero when computed in the opposite from HRV to the EEG components. No noticeable differences are detected in the values between pre- and post-ictal states, while a slight increase can be seen in the ictal phases; for a short period during the ictal event, the median GC from HRV to the EEG α component is comparable to the GC measured along the opposite direction (Fig. 3c). No evident lateralization effects of seizures are reported, as the GC values are similar if considering ipsilateral or contralateral brain activities.

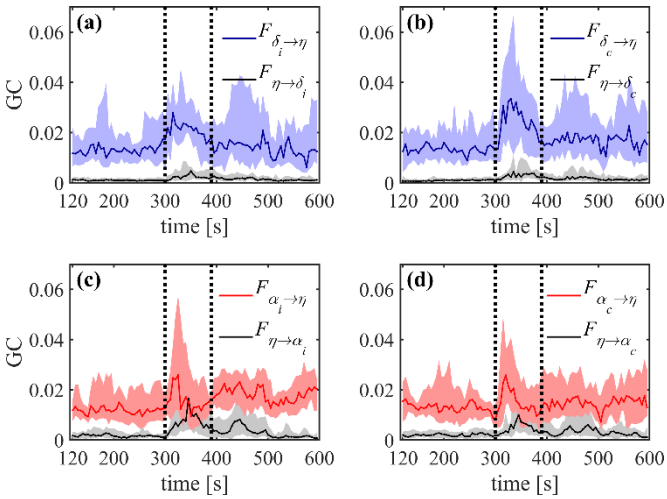

FIGURE 3. Bivariate measures of GC reflecting the directed interactions between HRV and the EEG components. (a) GC from the ipsilateral δ component to HRV (blue line) and from HRV to the ipsilateral δ component (grey line); (b) GC from the contralateral δ component to HRV (blue line) and from HRV to the contralateral δ component (grey line); (c) GC from the ipsilateral α component to HRV (red line) and from HRV to the ipsilateral α component (grey line); (d) GC from the ipsilateral α component to HRV (red line) and from HRV to the ipsilateral α component (grey line). In all panels, darker lines represent median values of the GC computed across subjects, while lighter color shades indicate 25th and 75th percentiles. Dotted lines delimit the ictal phase (median duration = 90 s). Values on the x-axis indicate the time at which the considered 120-s time-window ends.

Figure 4 shows the statistically significant values of the GC computed in both directions between HRV and the ipsilateral or contralateral δ and α EEG components for each considered 120-s time window; significance is assessed using the F-test applied to the residuals of the VAR model identified for each subject, and is reported counting the number of subjects for which the test was passed. Overall, the GC is highly significant when computed from the δ or α EEG components to HRV, while it is barely significant when computed in the

reverse direction from HRV to EEG components. These results are evident when considering $F_{\delta\to\eta}$ (significant in >10 subjects) and $F_{\eta\to\delta}$ (significant in <3 subjects), but hold also when considering $F_{\alpha\to\eta}$ (significant in >9 subjects) and $F_{\eta\to\alpha}$ (significant in <9 subjects). Similarly to what observed with regard to GC values, for a short period during the ictal event the significance of the GC from HRV to the EEG α component is comparable to that measured along the opposite direction.

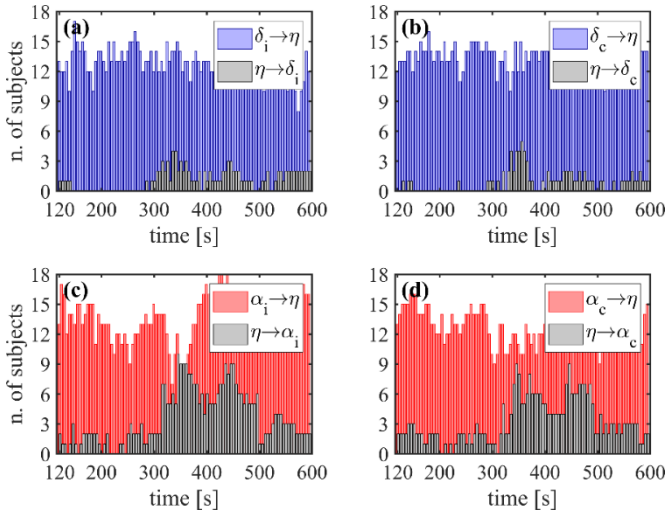

FIGURE 4. Number of subjects (out of 18) showing statistically significant bivariate measures of GC computed from the EEG δ component to HRV (blue bars) and from HRV to the EEG δ component (grey bars) considering ipsilateral (a) and contralateral (b) brain activities, and from the EEG α component to HRV (red bars) and from HRV to the EEG α component (grey bars) considering ipsilateral (c) and contralateral (d) brain activities. In all panels, each bar represents one of the 96 time windows, and values on the x-axis indicate the times at which the considered 120-s time window ends.

The absence of clear lateralization effects related to seizures is confirmed by the similar number of significant GC values for ipsilateral and contralateral EEG activities and by the lack of evident differences between pre-ictal and post-ictal states.

Figure 5 depicts the results of IID predictability analysis performed through trivariate VAR identification. Given the low and often non-significant values of the GC from HRV to the EEG components (see Figs. 3,4), IID predictability measures were computed only from the EEG components to HRV, according to the schematization in Fig. 2c. The JGC measure reported in Fig. 5a,b and the bivariate GC measures reported in Fig. 5c,e,d,f confirm the absence of visible differences between pre and post-ictal phases and between ipsilateral and contralateral activities. Interaction GC values are dominantly negative in all cases (Fig. 5g and 5h), evidencing that there is a prevalence of redundant interactions (see eq. (11)) between the ipsilateral and contralateral EEG activities in the prediction of HRV. While the IGC values are generally close to zero, a marked decrease is observed during the ictal phase for the α EEG activity (Fig. 5h) and especially for the δ activity (Fig. 5g).

Figure 6 depicts the results of PID predictability analysis performed through trivariate VAR identification. The synergistic predictability of HRV arising from the interaction between ipsilateral and contralateral EEG components displays rather stable values during the whole 10-min recording when assessed both for δ components (Fig. 6g) and for α components (Fig. 6h). The redundant predictability follows the trends of the IGC previously reported, increasing during the ictal phase especially when assessed from

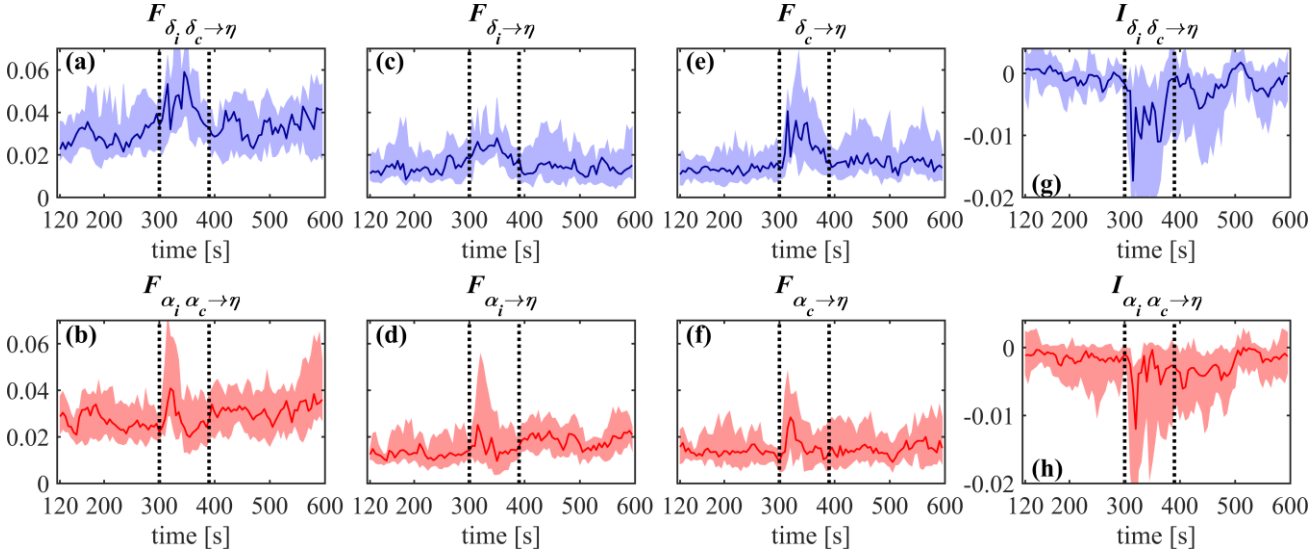

FIGURE 5. IID predictability decomposition for assessing the directed interactions from δ and α EEG components to HRV. (a,b) Joint GC from ipsilateral and contralateral EEG components to HRV; (c,d) bivariate GC from ipsilateral EEG components to HRV; (e,f) bivariate GC from contralateral EEG components to HRV; (g,h) interaction GC between ipsilateral and contralateral EEG to HRV. In all the panels, darker lines represent median values computed over all subjects, while lighter color shades indicate 25th and 75th percentiles. Dotted lines delimit the ictal phase. Values on the x-axis indicates the time at which the considered 120-s time-window ends.

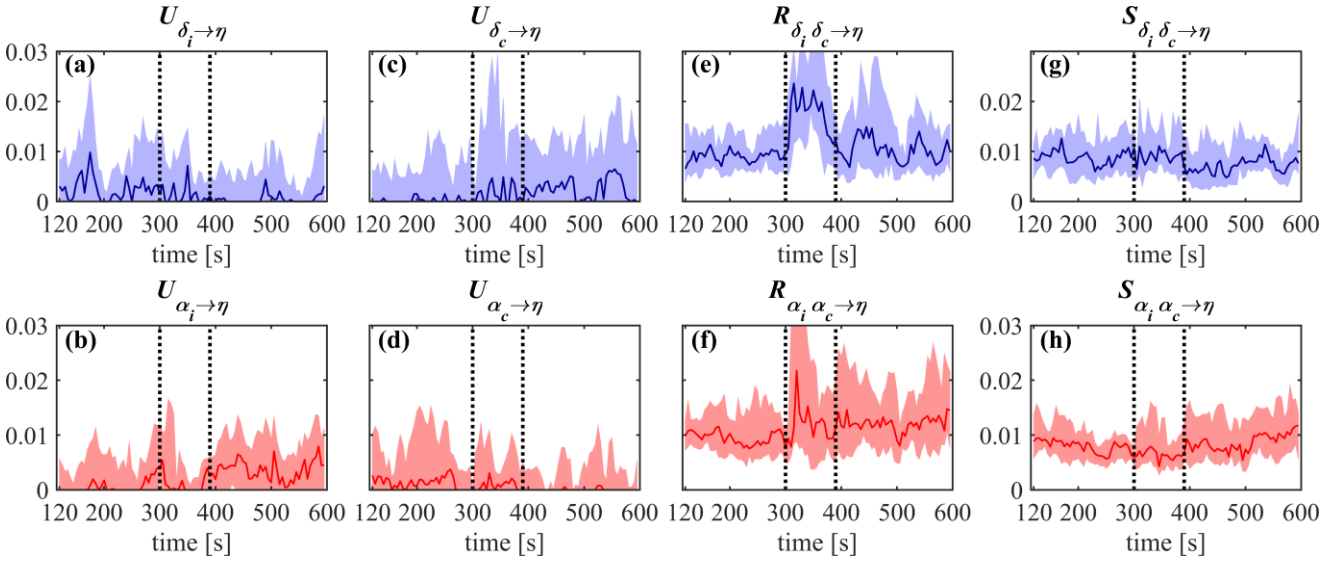

FIGURE 6. PID predictability decomposition for assessing the directed interactions from δ and α EEG components to HRV. (a,b) Unique GC from the ipsilateral EEG components to HRV; (c,d) Unique GC from the contralateral EEG components to HRV; (e,f) Redundant GC between the ipsilateral and contralateral EEG components to HRV; (g,h) Synergistic GC between the ipsilateral and contralateral EEG components to HRV. In all panels, darker lines represent median values computed over all subjects, while lighter color shades indicate 25th and 75th percentiles. Dotted lines delimit the ictal phase. Values on the x-axis indicate the time at which the considered 120-s time-window ends.

ipsilateral and contralateral δ EEG components to HRV (Fig. 6e). Both the synergistic and the redundant GC terms do not highlight clear seizure or lateralization effects. On the other hand, such effects are elicited using the unique predictability, which is built to be free from redundancy components. In detail, the results in Fig. 6a-d document that the unique predictability of HRV due to the δ EEG components originates mostly from the ipsilateral hemisphere during the pre-ictal phase (Fig. 6a), and mostly from the contralateral hemisphere during the post-ictal phase (Fig. 6c). An opposite result is observed for the α EEG components, with a prevalence of contralateral unique predictability before the seizure (Fig. 6d),

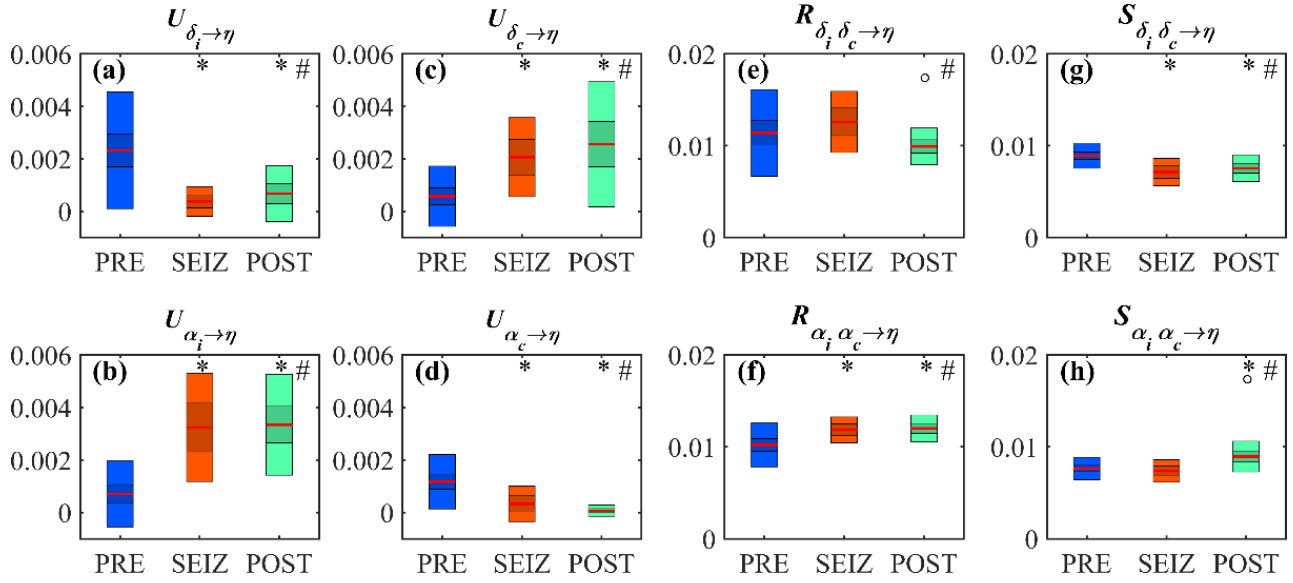

FIGURE 7. Boxplot distributions of the predictability measures obtained through PID computed during the pre-ictal (PRE, 48 windows, blue), ictal (SEIZ, 19 windows, orange) and post-ictal (POST, 28 windows, green) phases. (a,b) Unique GC from the ipsilateral EEG components to HRV; (c,d) Unique GC from the contralateral EEG components to HRV; (e,f) Redundant predictability between ipsilateral and contralateral EEG components to HRV; (g,h) Synergistic predictability between ipsilateral and contralateral EEG components to HRV. In all panels, red lines represent median values, darker and lighter color shades delimit one standard deviation and 95% confidence interval, respectively. Statistical tests: #; $p < 0:05$, Kruskal-Wallis test; * $p < 0.05$ PRE vs SEIZ or PRE vs POST; ° $p < 0.05$: SEIZ vs POST, pairwise Wilcoxon rank sum test with Bonferroni correction.

and a prevalence of ipsilateral unique predictability during and after the seizure (Fig. 6b).

The trends documented in Fig. 6 are supported by the statistical analysis whose results are reported in Fig. 7, showing the boxplot distributions of the predictability measures obtained through PID in the pre-ictal, ictal and post-ictal phases, and the results of statistical tests among conditions. The distributions represent the median values across all the subjects obtained for all the moving windows, according to the procedure described in Section 2. All the measures exhibit statistically significant variations across the three phases (Kruskal-Wallis test). The more evident variations regard the measures of unique predictability, which exhibit significant changes comparing the pre-ictal (PRE) phase with both ictal (SEIZ) and post-ictal (POST) phases for both δ and α EEG power and for both ipsilateral and contralateral electrodes (Fig. 7 a-d). In particular, the markedly lower values of $U_{\delta_i \to \eta}$ and $U_{\alpha_c \to \eta}$ and higher values of $U_{\delta_c \to \eta}$ and $U_{\alpha_i \to \eta}$ observed in the post-ictal compared with the pre-ictal phase confirm the opposite lateralization effects displayed by the EEG activity, i.e., HRV is driven by δ ipsilateral and α contralateral EEG components before the seizures, and by α ipsilateral and δ contralateral EEG components during and after the seizures. Moreover, the statistical analysis reveals that the redundant predictability between ipsilateral and contralateral α EEG increases significantly, and the synergistic predictability between ipsilateral and contralateral δ EEG decreases significantly, during the ictal and post-ictal phases compared with the pre-ictal phase (Fig. 7f and 7g). A tendency to significant increase of the synergistic α predictability and decrease of the redundant δ predictability is also observed in the post-ictal phase (Fig. 7h and 7e). As reported, most of the significant variations of the measures appear to be long-lasting, as suggested by the fact that pre-ictal values are not recovered in the post-ictal phase. The analyses were repeated using the same number of windows for all the three conditions, i.e. taking the first 19 windows in PRE and the last 19 in POST. The results highlight that all the statistically significant variations reported in Fig. 7 are still present, confirming that the statistical analysis carried out is robust w.r.t. the differences in the number of windows analyzed in each phase.

Discussion

The present work investigated pairwise and higher-order interactions among the dynamic processes that reflect the modulation of brain rhythms and cardiac autonomic activity associated with the development of temporal lobe epilepsy. Our methodology makes use of multivariate predictability measures to extend to higher-order interactions the well-known concept of Granger causality (GC). This approach allows to investigate the synergistic and redundant nature of the complex interactions between the epileptic network and the ANS, assessed respectively by the time series of the δ and α rhythms of the EEG recorded at regions placed ipsilaterally and contralaterally with respect to the epileptic focus, and by the time series of HRV measured from the ECG. The main methodological strength of our measures is that they are at the same time causal and multivariate, while for example classical pairwise GC measures do not address higher-order interactions, and the widely used CCM approach is limited to a bivariate implementation [31]. GC-based algorithms can assess the strength of the interactions separately for each direction, while other widely employed multivariate methods can reveal the strength of the coupling, but not the direction (see e.g. time delay stability [20] or multivariate correlation [26]). Moreover, the multivariate implementation whereby IID and PID measures are derived allows to take into account more processes, e.g. different brain waves and/or various biosignals, thus permitting to better describe the multi-faceted structure of interactions manifested within and between different physiological systems and in particular the combined effects that brain waves located in proximity and far away from seizure onset location have on HRV. At the same time, the implementation of IID and PID measures permits to separate the effects of different sources of predictability among processes and leads to quantify the exact amount of unique predictability between two processes [33]. The proposed measures also allow to isolate the contribute of a single hemisphere, either using classical bivariate approach where the EEG activity at one spatial location (ipsilateral or contralateral) is correlated with HRV, or through PID, computing the unique information transfer from the brain waves monitored at distinct scalp regions to the cardiac dynamics.

Application of the predictability framework has documented the clear prevalence of effects directed from brain to heart, with high and significant causal interactions from δ or α EEG components to HRV detected together low and barely significant interactions from HRV to δ or α (Figs. 3 and 4). Our results in terms of GC are very similar to those obtained through bivariate nonlinear CCM method on the same dataset, including also the temporary increase of the median GC from HRV to the EEG α component during the seizure event [31]. From a physiological point of view, these results indicate that the cortical activity drives ANS activity; similar interpretations were drawn in previous works on temporal lobe epilepsy in the children which analyzed EEG components and HRV through CCM method [17,31,51]. On the other hand, opposite directional effects between brain and heart dynamics deployed over whole-night recordings were found in Ref. [37] on healthy patients during sleep, where a predominance of heart-to-brain interactions was observed; this suggests that brain-heart interactions can occur in different forms across different physiological states and different time scales of observations.

In addition to the prevalence of interactions directed from brain to heart, the increased significance of GC values recorded during ictal and post-ictal phases (especially with regard to the α EEG power component) suggests that an alteration of the intensity of brain-to-heart effects takes place during the seizure, which is not recovered after few minutes and may thus be long-lasting. The increased interactions between the α EEG power component and HRV may be related to the shift in autonomic balance towards parasympathetic withdrawal and sympathetic dominance occurring during seizures that has been demonstrated in several studies focusing on the effects of epilepsy on HRV [2,3,62]. The variation of brain-heart interactions caused by seizures may be put in relation with the effects on ANS regulation already reported in the literature in terms of prolonged sympathetic overactivity and reduced HRV and baroreflex sensitivity [3,63]. Such changes in the ANS regulation have been considered important clinical biomarkers for the risk of SUDEP [2]. Moreover, we may also speculate that such changes in brain-heart interactions could be long-lasting, and thus may be related to the prolonged post-ictal symptoms already reported e.g. in [64] with cognitive changes lasting 30 to 60 minutes in adult patients with seizures originating in the frontal or temporal lobe, or in [65] where children suffering from focal seizures are more likely to experience postictal fatigue, sleepiness, or tiredness which affect their ability to return to normal activities.

The higher values of GC (see Figure 3(a) and (b)) and of joint GC (see Figure 5(a)) found during the seizures compared to other phases (especially the pre-ictal) may be put in relation to the increased δ brain activity in epileptic patients compared to healthy controls reported in [66]. The extent of δ activity has been considered in [66] as a diagnostic marker for recurrent seizures; moreover, it has also been speculated that the increased low frequency contribution to EEG in case of focal seizures could negatively affect memory processes and inhibit access to memory functions even without impairment of consciousness [67].

The GC measures alone were, however, not able to detect evident lateralization effects. This result is again in agreement with the application of CCM [31], which evidenced only marginal differences in the strength and direction of interactions between the cardiac dynamics and the EEG waves recorded at the sides of the brain ipsilateral and contralateral to the seizure location. A similar behavior has been emphasized - analyzing brain-brain interactions only- also by Lehnertz *et al.* [68] who indicated that in epileptic networks it remains to be shown whether the EEG dynamics of seizure onset zone can be characterized by an elevated strength of interactions. In Ref. [68], the inability to highlight lateralization effects was ascribed to the delay of interactions between and within brain regions, which should be taken into account by techniques explicitly incorporating time delays into information transfer estimates [68]. In our work we show that the use of PID predictability measures is the key to infer lateralization effects which are different before and after the epileptic seizure. In fact, the decomposition of the bivariate GC into unique and redundant measures of predictability allows to disambiguate the confounding effect of common EEG activities in the two brain hemispheres. In fact, our results suggest that the redundancy between ipsilateral and contralateral EEG activity precludes the detection of lateralization or temporal effects within the GC measures, and that such effects can be highlighted using the measures of unique predictability. Specifically, we find that the unique predictability $\delta \rightarrow \eta$ is mostly ipsilateral in the pre-ictal phase and contralateral in the post-ictal phase; an opposite pattern is reported for the unique predictability $\alpha \rightarrow \eta$, which prevails at contralateral sites before the seizures and at ipsilateral sites after the seizures. This evidences the strong effect of epileptic seizures, which change the interaction patterns present in the pre-ictal phase to a different one, not only nearby the seizure onset zone, but also in the opposite hemisphere. These findings documenting the complexity of brain-heart interactions related to epilepsy support the well-recognized concept of "epileptic ensemble or network" which is more complex and heterogeneous than previously thought, with effects reported far from the seizure onset location [68,69] even in case of focal events. Moreover, the derivation of high-order interaction measures specific of ipsilateral and/or contralateral information transfer may be in perspective useful to the classification of focal seizures based on non-invasive biosignal recordings.

The present study assessed brain-heart interactions using linear parametric methods, which have been shown as appropriate to analyze dynamic brain-heart interactions [5,20,56,70,71]. Nonetheless, future analyses should employ nonlinear and model-free PID formulations, which may be able to evidence further contributions brought by nonlinear dynamics to brain-heart interactions; these extensions should consider that current formulations of model-free measures still tend to yield highly-biased measures and pose severe constraints on data length and possibly temporal resolution [71–74]. A limitation of our work is that analyses have been carried out on EEG scalp signals, which are usually affected by volume conduction effects, or by confounding factors e.g. due to the by superposition of underlying brain source activities [31,75]. Nonetheless, time series extracted from scalp EEG recordings still represent a valid starting point for investigating on brain network interactions, even if more reliable results may be obtained in a future work using, instead than more invasive depth electrodes, frameworks for reconstructing source signals [75,76]. Moreover, several works demonstrated that the selection of the EEG reference can have a fundamental impact on the signal of interest [77–79]. In this sense, a recent study evidenced the importance of

investigating different choices for the reference electrode with specific regard to the evaluation of brain-heart interactions, suggesting that the common average reference (i.e. potentials measured in the EEG dataset averaged across the whole scalp) could be more suitable than a specific physical reference; this aspect should be investigated in later studies. Further extensions of our study should take into account inter-ictal periods, e.g. to confirm whether the changes in brain-heart interactions provoked by seizures and detected in our study effectively represent long-lasting effects. Moreover, while in this work we have just taken into account the two electrodes which characterize best the focus area of temporal lobe epilepsy starting from the recorded EEG activities both before, during and after the seizure, it would be also noteworthy to carry out a more detailed investigation of the involvement of other (multiple) electrodes in later studies. Future works should also consider different classes of epileptic patients, e.g. comparing the effects on brain-heart interactions of focal and generalized seizures [3] to assess the seizure classification ability of the proposed measures, and datasets obtained from healthy subjects, e.g. to test whether the absence of directed interactions from heart to brain observed in this work is a peculiarity of epilepsy rather than a general feature of brain-heart interactions.

Conclusion

The present work highlights the importance of applying multivariate predictability measures able to quantify both pairwise and higher-order effects in order to elicit region-specific contributions to brain-heart interactions in the analysis of the complex coupling between the epileptic network and the ANS in children with TLE.

Our results document the existence of different patterns of brain-to-heart predictability depending on the input signals (δ or α brain waves), temporal information (pre-, during- or post-ictal) and spatial constraints (ipsilateral or contralateral) relevant to the study of EEG-HRV interactions. From a physiological perspective, we have highlighted (i) the prevalence of efferent physiological interactions from the cortex to the sinus node, and (ii) that epileptic seizures swap the frequency of the brain waves driving such interactions (i.e., in areas close to the epileptic focus, brain-to-heart interactions are driven by the δ waves before the seizure, and by the α waves after the seizure).

The proposed approach may help the elucidation of the neuroautonomic effects of TLE, and in perspective may have clinical implications for the treatment of focal epilepsy. Future studies should assess the generality of these findings as regards the characterization of brain-body interactions in the field of Network Physiology.

Funding

RP was supported by the Italian MIUR PON R&I 2014-2020 AIM project no. AIM1851228-2. LF was supported by the Italian MIUR PRIN 2017 project 2017WZFTZP “Stochastic forecasting in complex systems”.

Ethical statement

The protocol was approved by the local ethical committee of the University Hospital of Vienna.

References

[1] Fisher R S, Boas W van E, Blume W, Elger C, Genton P, Lee P and Engel J 2005 Epileptic Seizures and Epilepsy: Definitions Proposed by the International League Against Epilepsy (ILAE) and the International Bureau for Epilepsy (IBE) *Epilepsia* **46** 470–2

[2] Lotufo P A, Valiengo L, Benseñor I M and Brunoni A R 2012 A systematic review and meta-analysis of heart rate variability in epilepsy and antiepileptic drugs *Epilepsia* **53** 272–82

[3] Pernice R, Faes L, Kotiuchyi I, Stivala S, Busacca A, Popov A and Kharytonov V 2019 Time, frequency and information domain analysis of short-term heart rate variability before and after focal and generalized seizures in epileptic children *Physiol. Meas.* **40** 74003

[4] Smith S J M 2005 EEG in the diagnosis, classification, and management of patients with epilepsy *J. Neurol. Neurosurg. Psychiatry* **76 Suppl 2** ii2–7

[5] Piper D, Schiecke K, Pester B, Benninger F, Feucht M and Witte H 2014 Time-variant coherence between heart rate variability and EEG activity in epileptic patients: an advanced coupling analysis between physiological networks *New J. Phys.* **16** 115012

[6] Centeno M and Carmichael D W 2014 Network connectivity in epilepsy: resting state fMRI and EEG–fMRI contributions *Front. Neurol.* **5** 93

[7] Pereira F R S, Alessio A, Sercheli M S, Pedro T, Bilevicius E, Rondina J M, Ozelo H F B, Castellano G, Covolan R J M and Damasceno B P 2010 Asymmetrical hippocampal connectivity in mesial temporal lobe epilepsy: evidence from resting state fMRI *BMC Neurosci.* **11** 1–13

[8] Shaffer F and Ginsberg J P 2017 An Overview of Heart Rate Variability Metrics and Norms *Front. public Heal.* **5** 258

[9] Malik M, Bigger J T, Camm A J, Kleiger R E, Malliani A, Moss A J and Schwartz P J 1996 Heart rate variabilityStandards of measurement, physiological interpretation, and clinical use *Eur. Heart J.* **17** 354–81

[10] Pernice R, Javorka M, Krohova J, Czippelova B, Turianikova Z, Busacca A and Faes L 2019 Comparison of short-term heart rate variability indexes evaluated through electrocardiographic and continuous blood pressure monitoring *Med. Biol. Eng. Comput.* **57** 1247–63

[11] Valenza G, Toschi N and Barbieri R 2016 Uncovering brain–heart information through advanced signal and image processing

[12] Silvani A, Calandra-Buonaura G, Dampney R A L and Cortelli P 2016 Brain–heart interactions: physiology and clinical implications *Philos. Trans. R. Soc. A Math. Phys. Eng. Sci.* **374** 20150181

[13] Catrambone V and Valenza G 2021 *Functional Brain-Heart Interplay* (Springer)

[14] Greco A, Faes L, Catrambone V, Barbieri R, Scilingo E P and Valenza G 2019 Lateralization of directional brain-heart information transfer during visual emotional elicitation *Am. J. Physiol. Integr. Comp. Physiol.* **317** R25–38

[15] Costagliola G, Orsini A, Coll M, Brugada R, Parisi P and Striano P 2021 The brain–heart interaction in epilepsy: implications for diagnosis, therapy, and SUDEP prevention *Ann. Clin. Transl. Neurol.*

[16] Bahari F, Ssentongo P, Schiff S J and Gluckman B J 2018 A brain–heart biomarker for epileptogenesis *J. Neurosci.* **38** 8473–83

[17] Schiecke K, Schumann A, Benninger F, Feucht M, Baer K-J and Schlattmann P 2019 Brain–heart interactions considering complex physiological data: processing schemes for time-variant, frequency-dependent, topographical and statistical examination of directed interactions by convergent cross mapping *Physiol. Meas.* **40** 114001

[18] Schiecke K, Wacker M, Piper D, Benninger F, Feucht M and Witte H 2014 Time-variant, frequency-selective, linear and nonlinear analysis of heart rate variability in children with temporal lobe epilepsy *IEEE Trans. Biomed. Eng.* **61** 1798–808

[19] Van der Lende M, Surges R, Sander J W and Thijs R D 2016 Cardiac arrhythmias during or after epileptic seizures *J. Neurol. Neurosurg. Psychiatry* **87** 69–74

[20] Bartsch R P, Liu K K L, Bashan A and Ivanov P C 2015 Network Physiology: How Organ Systems Dynamically Interact *PLoS One* **10** e0142143

[21] Ivanov P C, Liu K K L and Bartsch R P 2016 Focus on the emerging new fields of network physiology and network medicine *New J. Phys.* **18** 100201

[22] Candia-Rivera D, Catrambone V, Thayer J F, Gentili C and Valenza G 2022 Cardiac sympathetic-vagal activity initiates a functional brain–body response to emotional arousal *Proc. Natl. Acad. Sci.* **119** e2119599119

[23] Catrambone V and Valenza G 2021 BHI estimation methodology *Functional Brain-Heart Interplay* (Springer) pp 21–50

[24] Kim D-K, Lee K-M, Kim J, Whang M-C and Kang S W 2013 Dynamic correlations between heart and brain rhythm during Autogenic meditation *Front. Hum. Neurosci.* **7** 414

[25] Lin P-F, Lo M-T, Tsao J, Chang Y-C, Lin C and Ho Y-L 2014 Correlations between the signal complexity of cerebral and cardiac electrical activity: a multiscale entropy analysis *PLoS One* **9** e87798

[26] Pernice R, Antonacci Y, Zanetti M, Busacca A, Marinazzo D, Faes L and Nollo G 2021 Multivariate Correlation Measures Reveal Structure and Strength of Brain–Body Physiological Networks at Rest and During Mental Stress *Front. Neurosci.* **14** 1427

[27] Dumont M, Jurysta F, Lanquart J-P, Migeotte P-F, Van De Borne P and Linkowski P 2004 Interdependency between heart rate variability and sleep EEG: linear/non-linear? *Clin. Neurophysiol.* **115** 2031–40

[28] Catrambone V and Valenza G 2021 Sympathovagal Changes *Functional Brain-Heart Interplay* (Springer) pp 53–78

[29] Bari V, Marchi A, De Maria B, Rossato G, Nollo G, Faes L and Porta A 2016 Nonlinear effects of respiration on the crosstalk between cardiovascular and cerebrovascular control systems *Philos. Trans. R. Soc. A Math. Phys. Eng. Sci.* **374** 20150179

[30] Catrambone V, Greco A, Vanello N, Scilingo E P and Valenza G 2019 Time-Resolved Directional Brain–Heart Interplay Measurement Through Synthetic Data Generation Models *Ann. Biomed. Eng.* **47** 1479–89

[31] Schiecke K, Pester B, Piper D, Benninger F, Feucht M, Leistritz L and Witte H 2016 Nonlinear Directed Interactions Between HRV and EEG Activity in Children With TLE *IEEE Trans. Biomed. Eng.* **63** 2497–504

[32] Faes L, Porta A, Nollo G and Javorka M 2017 Information Decomposition in Multivariate Systems: Definitions, Implementation and Application to Cardiovascular Networks *Entropy* **19**

[33] Faes L, Marinazzo D and Stramaglia S 2017 Multiscale Information Decomposition: Exact Computation for Multivariate Gaussian Processes *Entropy* **19**

[34] Krohova J, Faes L, Czippelova B, Turianikova Z, Mazgutova N, Pernice R, Busacca A, Marinazzo D, Stramaglia S and Javorka M 2019 Multiscale Information Decomposition Dissects Control Mechanisms of Heart Rate Variability at Rest and During Physiological Stress *Entropy* **21**

[35] Faes L, Nollo G and Porta A 2011 Information-based detection of nonlinear Granger causality in multivariate processes via a nonuniform embedding technique *Phys. Rev. E* **83** 51112

[36] Porta A, Guzzetti S, Montano N, Pagani M, Somers V, Malliani A, Baselli G and Cerutti S 2000 Information domain analysis of cardiovascular variability signals: evaluation of regularity, synchronisation and co-ordination *Med. Biol. Eng. Comput.* **38** 180–8

[37] Faes L, Marinazzo D, Jurysta F and Nollo G 2015 Linear and non-linear brain–heart and brain–brain interactions during sleep *Physiol. Meas.* **36** 683

[38] Faes L, Porta A, Rossato G, Adami A, Tonon D, Corica A and Nollo G 2013 Investigating the mechanisms of cardiovascular and cerebrovascular regulation in orthostatic syncope through an information decomposition strategy *Auton. Neurosci. Basic Clin.* **178** 76–82

[39] Zanetti M, Faes L, Nollo G, De Cecco M, Pernice R, Maule L, Pertile M and Fornaser A 2019 Information Dynamics of the Brain, Cardiovascular and Respiratory Network during Different Levels of Mental Stress *Entropy* **21**

[40] Granger C W J 1969 Investigating causal relations by econometric models and cross-spectral methods *Econom. J. Econom. Soc.* 424–38

[41] Barrett A B, Barnett L and Seth A K 2010 Multivariate Granger causality and generalized variance *Phys. Rev. E* **81** 41907

[42] Nuzzi D, Stramaglia S, Javorka M, Marinazzo D, Porta A and Faes L 2021 Extending the spectral decomposition of Granger causality to include instantaneous influences: application to the control mechanisms of heart rate variability *Philos. Trans. R. Soc. A* **379** 20200263

[43] Battiston F, Cencetti G, Iacopini I, Latora V, Lucas M, Patania A, Young J-G and Petri G 2020 Networks beyond pairwise interactions: structure and dynamics *Phys. Rep.*

[44] Antonacci Y, Minati L, Nuzzi D, Mijatovic G, Pernice R, Marinazzo D, Stramaglia S and Faes L 2021 Measuring High-Order Interactions in Rhythmic Processes through Multivariate Spectral Information Decomposition *IEEE Access*

[45] Rosas F E, Mediano P A M, Luppi A I, Varley T F, Lizier J T, Stramaglia S, Jensen H J and Marinazzo D 2022 Disentangling high-order mechanisms and high-order behaviours in complex systems *Nat. Phys.* **18** 476–7

[46] Stramaglia S, Scagliarini T, Daniels B C and Marinazzo D 2021 Quantifying dynamical high-order interdependencies from the o-information: an application to neural spiking

dynamics *Front. Physiol.* **11** 1784
[47] Chua K C, Chandran V, Acharya U R and Lim C M 2010 Application of higher order statistics/spectra in biomedical signals—A review *Med. Eng. Phys.* **32** 679–89
[48] Khoshnevis S A and Sankar R 2019 Applications of higher order statistics in electroencephalography signal processing: A comprehensive survey *IEEE Rev. Biomed. Eng.* **13** 169–83
[49] Catrambone V, Barbieri R, Wendt H, Abry P and Valenza G 2021 Functional brain–heart interplay extends to the multifractal domain *Philos. Trans. R. Soc. A* **379** 20200260
[50] Lizier J T, Bertschinger N, Jost J and Wibral M 2018 Information decomposition of target effects from multi-source interactions: Perspectives on previous, current and futurework *Entropy* **20**
[51] Schiecke K, Benninger F and Feucht M 2021 Analysis of Brain-Heart Couplings in Epilepsy: Dealing With the Highly Complex Structure of Resulting Interaction Pattern *2020 28th European Signal Processing Conference (EUSIPCO)* (IEEE) pp 935–9
[52] Mayer H, Benninger F, Urak L, Plattner B, Geldner J and Feucht M 2004 EKG abnormalities in children and adolescents with symptomatic temporal lobe epilepsy *Neurology* **63** 324–8
[53] French A S and Holden A V 1971 Alias-free sampling of neuronal spike trains *Kybernetik* **8** 165–71
[54] Rehman N and Mandic D P 2010 Multivariate empirical mode decomposition *Proc. R. Soc. A Math. Phys. Eng. Sci.* **466** 1291–302
[55] Goebel R, Roebroeck A, Kim D-S and Formisano E 2003 Investigating directed cortical interactions in time-resolved fMRI data using vector autoregressive modeling and Granger causality mapping *Magn. Reson. Imaging* **21** 1251–61
[56] Faes L, Marinazzo D, Stramaglia S, Jurysta F, Porta A and Giandomenico N 2016 Predictability decomposition detects the impairment of brain–heart dynamical networks during sleep disorders and their recovery with treatment *Philos. Trans. R. Soc. A Math. Phys. Eng. Sci.* **374** 20150177
[57] Barrett A B 2015 Exploration of synergistic and redundant information sharing in static and dynamical Gaussian systems *Phys. Rev. E* **91** 52802
[58] Faes L, Porta A and Nollo G 2015 Information decomposition in bivariate systems: theory and application to cardiorespiratory dynamics *Entropy* **17** 277–303
[59] Faes L, Stramaglia S and Marinazzo D 2017 On the interpretability and computational reliability of frequency-domain Granger causality *F1000Research* **6**
[60] Montalto A, Faes L and Marinazzo D 2014 MuTE: a MATLAB toolbox to compare established and novel estimators of the multivariate transfer entropy *PLoS One* **9** e109462
[61] Bressler S L and Seth A K 2011 Wiener–Granger causality: a well established methodology *Neuroimage* **58** 323–9
[62] Jansen K and Lagae L 2010 Cardiac changes in epilepsy *Seizure* **19** 455–60
[63] Esmaeili B, Kaffashi F, Theeranaew W, Dabir A, Lhatoo S D and Loparo K A 2018 Post-ictal modulation of baroreflex sensitivity in patients with intractable epilepsy *Front. Neurol.* **9** 793
[64] Helmstaedter C, Elger C E and Lendt M 1994 Postictal courses of cognitive deficits in focal epilepsies *Epilepsia* **35** 1073–8
[65] MacEachern S J, D'Alfonso S, McDonald R J, Thornton N, Forkert N D and Buchhalter J R 2017 Most children with epilepsy experience postictal phenomena, often preventing a return to normal activities of childhood *Pediatr. Neurol.* **72** 42–50
[66] Schönherr M, Stefan H, Hamer H M, Rössler K, Buchfelder M and Rampp S 2017 The delta between postoperative seizure freedom and persistence: automatically detected focal slow waves after epilepsy surgery *NeuroImage Clin.* **13** 256–63
[67] Höller Y and Trinka E 2015 Is there a relation between EEG-slow waves and memory dysfunction in epilepsy? A critical appraisal *Front. Hum. Neurosci.* **9** 341
[68] Lehnertz K and Dickten H 2015 Assessing directionality and strength of coupling through symbolic analysis: an application to epilepsy patients *Philos. Trans. R. Soc. A Math. Phys. Eng. Sci.* **373** 20140094
[69] Bower M R, Stead M, Meyer F B, Marsh W R and Worrell G A 2012 Spatiotemporal neuronal correlates of seizure generation in focal epilepsy *Epilepsia* **53** 807–16
[70] Faes L, Nollo G, Jurysta F and Marinazzo D 2014 Information dynamics of brain-heart physiological networks during sleep *New J. Phys.* **16** 105005
[71] Duggento A, Bianciardi M, Passamonti L, Wald L L, Guerrisi M, Barbieri R and Toschi N 2016 Globally conditioned Granger causality in brain–brain and brain–heart interactions: a combined heart rate variability/ultra-high-field (7 T) functional magnetic resonance imaging study *Philos. Trans. R. Soc. A Math. Phys. Eng. Sci.* **374** 20150185
[72] Runge J, Heitzig J, Petoukhov V and Kurths J 2012 Escaping the curse of dimensionality in estimating multivariate transfer entropy *Phys. Rev. Lett.* **108** 258701
[73] Faes L, Kugiumtzis D, Nollo G, Jurysta F and Marinazzo D 2015 Estimating the decomposition of predictive information in multivariate systems *Phys. Rev. E* **91** 32904
[74] Faes L, Nollo G and Chon K H 2008 Assessment of Granger causality by nonlinear model identification: application to short-term cardiovascular variability *Ann. Biomed. Eng.* **36** 381–95
[75] Van de Steen F, Faes L, Karahan E, Songsiri J, Valdes-Sosa P A and Marinazzo D 2019 Critical Comments on EEG Sensor Space Dynamical Connectivity Analysis *Brain Topogr.* **32** 643–54
[76] Kotiuchyi I, Pernice R, Popov A, Faes L and Kharytonov V 2020 A framework to assess the information dynamics of source EEG activity and its application to epileptic brain networks *Brain Sci.* **10** 1–23
[77] Kayser J and Tenke C E 2010 In search of the Rosetta Stone for scalp EEG: converging on reference-free techniques *Clin. Neurophysiol. Off. J. Int. Fed. Clin. Neurophysiol.* **121** 1973
[78] Hagemann D, Naumann E and Thayer J F 2001 The quest for the EEG reference revisited: A glance from brain asymmetry research *Psychophysiology* **38** 847–57
[79] Candia-Rivera D, Catrambone V and Valenza G 2021 The role of electroencephalography electrical reference in the assessment of functional brain–heart interplay: From methodology to user guidelines *J. Neurosci. Methods* **360** 109269